applied sciences

MDPI

Article

From Measured In Situ Stress to Dynamic Simulation: A Calibrated 3DEC Model of a Rock Quarry

Vivien De Lucia [1,*], Domenico Gullì [2], Daria Marchetti [2] and Riccardo Salvini [1,*]

[1] Department of Physical Sciences, Earth and Environment, Centre of Geotechnologies CGT, University of Siena, 52027 San Giovanni Valdarno, Italy
[2] USL Toscana Nord-Ovest, UOC Ingegneria Mineraria, Tuscany Region, 54033 Carrara, Italy
* Correspondence: vivien.delucia2@unisi.it (V.D.L.); riccardo.salvini@unisi.it (R.S.)

Abstract

Accurately reproducing the mechanical and dynamic behavior of fractured rock masses remains a key challenge in rock engineering, especially in marble quarry environments where discontinuity networks, excavation geometry, and topographic effects induce highly nonlinear stress distributions. This study presents a multidisciplinary and physically calibrated numerical approach integrating field stress measurements, structural characterization, and dynamic modeling using the Distinct Element Method (DEM). The analysis focuses on a marble quarry located in the Apuan Alps (Italy), a tectonically complex metamorphic massif characterized by intense deformation and pervasive jointing that strongly influence rock mass behavior under both static and seismic loading. The initial stress field was calibrated using in situ measurements obtained by the CSIRO Hollow Inclusion technique, enabling reconstruction of the three-dimensional principal stress regime and its direct incorporation into a 3DEC numerical model. The calibrated model was then employed to simulate the dynamic response of the rock mass under seismic loading consistent with the Italian Building Code (NTC 2018). This coupled static–dynamic workflow provides a realistic evaluation of ground motion amplification, stress concentration, and potential failure mechanisms along pre-existing discontinuities. Results demonstrate that physically validated stress initialization yields a significantly more realistic response than models based on simplified lithostatic or empirical assumptions. The approach highlights the value of integrating geological, geotechnical, and seismological data into a unified modeling framework for a sustainable quarry stability analysis in fractured rock masses.

Keywords: Distinct Element Method (DEM); 3DEC numerical simulation; in situ stress calibration; seismic response; quarry stability assessment

Academic Editors: Junwei Chen, Zhi Zhao and Jian-Zhi Zhang

Received: 19 November 2025
Revised: 3 December 2025
Accepted: 8 December 2025
Published: 12 December 2025

Citation: De Lucia, V.; Gullì, D.; Marchetti, D.; Salvini, R. From Measured In Situ Stress to Dynamic Simulation: A Calibrated 3DEC Model of a Rock Quarry. *Appl. Sci.* **2025**, *15*, 13100. https://doi.org/10.3390/app152413100

1. Introduction

Fractured rock masses represent some of the most complex and heterogeneous systems in geotechnical and mining engineering [1]. Their mechanical behavior—especially under dynamic or excavation-induced loading—emerges from the intricate interaction between intact rock, discontinuities, and the in situ stress field [2,3]. Understanding and predicting these coupled processes is fundamental for ensuring the long-term stability and safety of large underground and open-pit excavations such as tunnels, quarries, and mines [4,5].

Over the past few decades, significant advances in the numerical modeling of fractured rock systems have been achieved using Distinct Element Methods (DEM), that explicitly represent discontinuities and the resulting block interactions [6,7]. DEM-based software

such as Itasca 3DEC [8] has proven particularly effective in simulating stress and displacement distributions, block detachment, and dynamic wave propagation within jointed rock masses [9,10]. However, despite these capabilities, a fundamental limitation persists: the initial stress state is often assumed rather than directly measured, introducing substantial uncertainty into model predictions [11].

The knowledge of the in situ stress field is crucial to the reliability of both static and dynamic simulations [12,13]. Simplified assumptions—such as lithostatic gradients or uniform horizontal-to-vertical stress ratios—may be convenient, yet they fail to capture the spatial variability of stresses induced by geological structures, excavation geometry, and topography [14,15]. This limitation becomes particularly critical in marble quarries, where anisotropic mechanical behavior, strong structural control, and irregular excavation geometries generate complex stress distributions even prior to any dynamic loading [16,17].

To overcome these limitations, contemporary research increasingly emphasizes the integration of direct field measurements into numerical modeling workflows. Among available techniques, the Commonwealth Scientific and Industrial Research Organization - Hollow Inclusion (CSIRO HI) method stands out for its ability to provide three-dimensional in situ stress tensors [18–20] with minimal disturbance to the rock mass. When coupled with DEM-based analyses, these data enable the reconstruction of the actual stress regime, offering a physically calibrated foundation for numerical modeling. This integration marks a shift from theoretical modeling toward physically validated simulations, in which both geometry and stress conditions are grounded in field evidence rather than idealized assumptions [21,22].

Within this methodological framework, the Carrara marble district in the Apuan Alps (Tuscany, Italy) provides an exceptional natural laboratory. It is one of the world's most intensively exploited dimension-stone regions, where extraction activities are increasingly shifting underground due to environmental and landscape constraints. This transition has renewed the need for robust geomechanical modeling, as underground excavation demands a precise understanding of the stress regime and its role in controlling excavation stability. Safety concerns are particularly relevant in such environments, where stress redistribution in fractured carbonate rocks can induce localized failures in chambers, pillars, and quarry fronts [23,24].

Traditional stability assessments in Carrara have mainly relied on empirical rock mechanics testing and structural mapping [25,26]. Although valuable, these approaches have limitations when applied to highly discontinuous and anisotropic rock masses, where stress interactions depend strongly on excavation geometry. Recent research has thus demonstrated the benefits of integrating advanced remote sensing techniques—such as terrestrial laser scanning (TLS), UAV (Unmanned Aerial Vehicle) photogrammetry, and airborne LiDAR (Light Detection and Ranging)—with numerical simulations to produce accurate three-dimensional reconstructions of quarry geometry. When combined with in situ stress measurements, this approach allows for the physical calibration of numerical models, improving both accuracy and predictive reliability [27,28].

Building upon these advances, the present study aims at applying a multidisciplinary and physically validated numerical workflow to the Ravalunga quarry, located within the Colonnata basin of Carrara. The methodology combines CSIRO HI overcoring tests, in situ compression tests, high-resolution remote sensing (TLS, UAV photogrammetry, LiDAR), and three-dimensional DEM modeling using 3DEC v7. This integrated dataset may allow the construction of a fully calibrated digital model of the quarry, capable of simulating both static and dynamic conditions under realistic stress fields.

Beyond the specific case study, this research underscores the broader methodological importance of unifying geological, geotechnical, and seismological data in a consistent

modeling framework. By coupling field-calibrated stress data with dynamic DEM simulations, the study advances a physically based approach to the analysis of seismic response and excavation stability in fractured rock masses. Such a framework not only enhances the reliability of numerical predictions but also contributes to sustainable resource extraction and hazard mitigation in complex geological settings worldwide.

2. Study Area

The Ravalunga quarry is located within the Colonnata extraction basin, in the central sector of the Carrara marble district (Figure 1). The site lies on the right hydrographic side of the Fossa al Canalone stream, below the ridge connecting Monte Maggiore (1390 m a.s.l.), Cima Canal Grande (1274 m a.s.l.), and Monte Serrone (1063 m a.s.l.). This topographic framework is representative of the steep alpine morphology typical of the northern Apuan chain, where deep valleys and high ridges exert strong control on local stress orientations and slope stability [29,30].

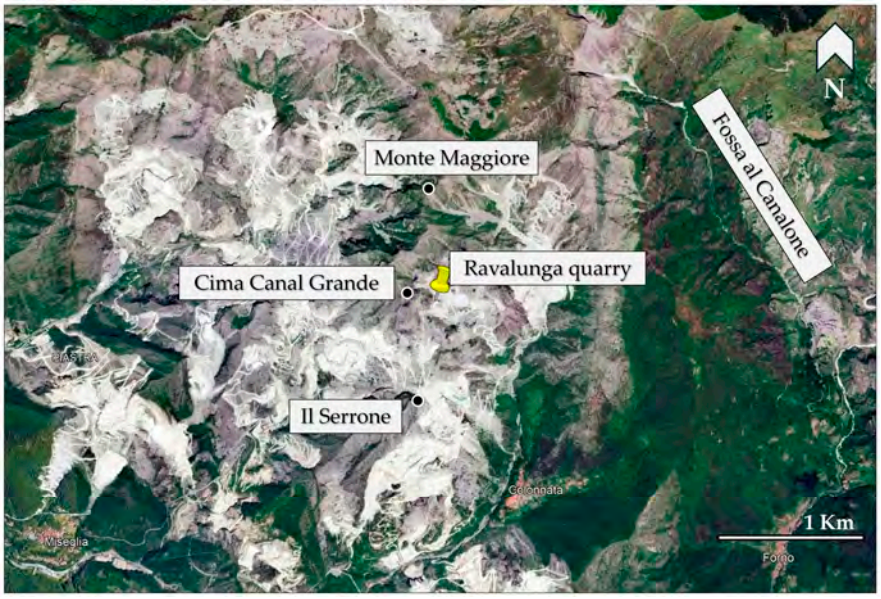

Figure 1. Apuan Alps marble district. The yellow pin indicates the location of the quarry n.138 Ravalunga.

Historically, Ravalunga was exploited primarily as an open-pit quarry, later evolving toward underground extraction. The open-pit quarry develops across two main working yards (Figure 2): a southern lower yard at approximately 1016.5 m a.s.l. and a northern upper yard around 1078 m a.s.l. [29]. These two sectors are separated by the natural gully known as the Fossa di Ravalunga, a right-bank tributary of the Fossa al Canalone stream, which marks the central morphological boundary of the site and has influenced the geometry of quarry development. The southwestern quarry front exposes residual marble walls reaching a maximum height of about 120 m, locally characterized by discontinuous and partially weathered structural surfaces.

The access road, ascending from the valley across the main quarry debris, and the service platform at ~1020 m a.s.l., used for temporary storage of blocks and waste material, are both structurally stable and functional for current operations. The underground excavation lies southeast of the open-pit fronts, along the extension of the access road. Access to the underground tunnel is via an entrance tunnel located at 980 m a.s.l (Figure 2).

From a geological perspective, the quarry is located within the metamorphic core of the Apuan Alps (Figure 3), where the Carrara Marble Formation—a thick succession of coarse-grained calcite marbles belonging to the Apuan Unit—is affected by a dense

network of NW–SE and NE–SW trending discontinuities, i.e., joints, faults, and stylolitic bands [31]. The rock mass is typically anisotropic, with mechanical properties strongly influenced by both the spacing and persistence of discontinuities.

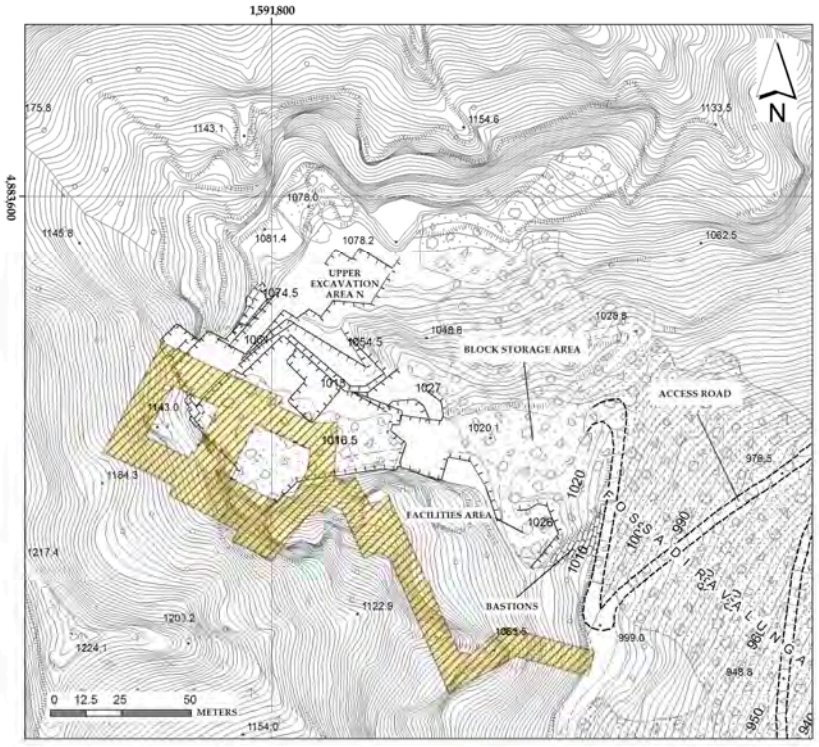

Figure 2. Plan view of the Ravalunga quarry area (modified from [29]). The yellow area indicates the underground tunnel.

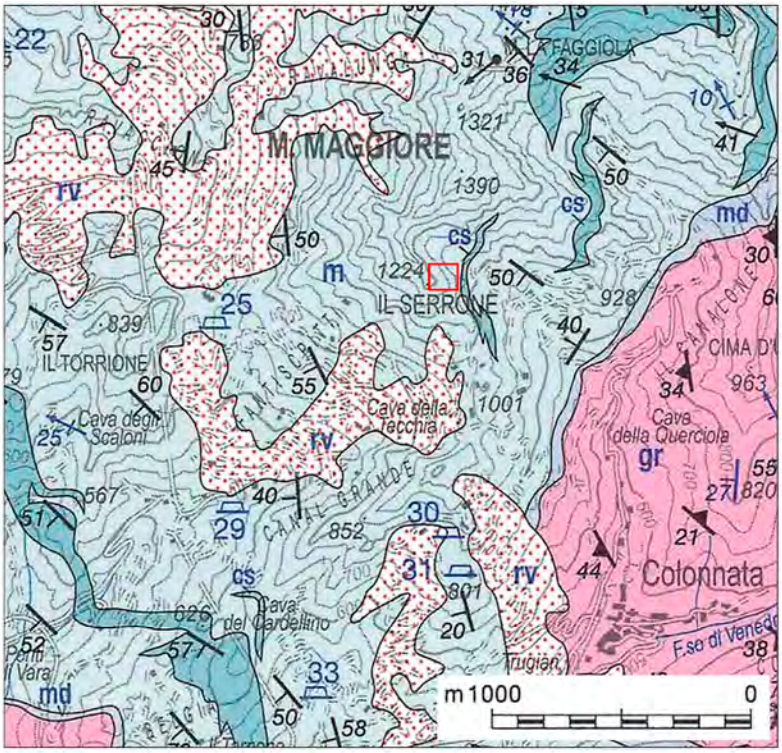

Figure 3. Geological map of the study area; the red square shows the location of the quarry. Abbreviations: cs = cherty metalimestone; m = marble; md = dolomitic marble; gr = dolomite ("grezzoni"); rv = quarry debris ("ravaneto").

3. Materials and Methods

3.1. Topographic Survey and 3D Model Generation

A detailed topographic survey of the Ravalunga quarry was conducted with the aim of obtaining a 3D representation of the site geometry. Initial topographic data for the study area was provided by the quarry property, and it was integrated with new surveys conducted by the authors, particularly in the underground sector, to acquire updated morphological features of the site. For the open-pit portion of the quarry, data was acquired using UAV photogrammetry, while the underground excavation was surveyed by TLS. These complementary datasets were merged to generate a dense 3D point cloud (over 14 million points) that provides a detailed and accurate reconstruction of the entire quarry geometry (Figure 4). All spatial data were georeferenced in the Italian national Gauss–Boaga coordinate system (Western Zone) to ensure a consistent reference frame for subsequent analyses thanks to a Global Navigation Satellite System (GNSS) survey.

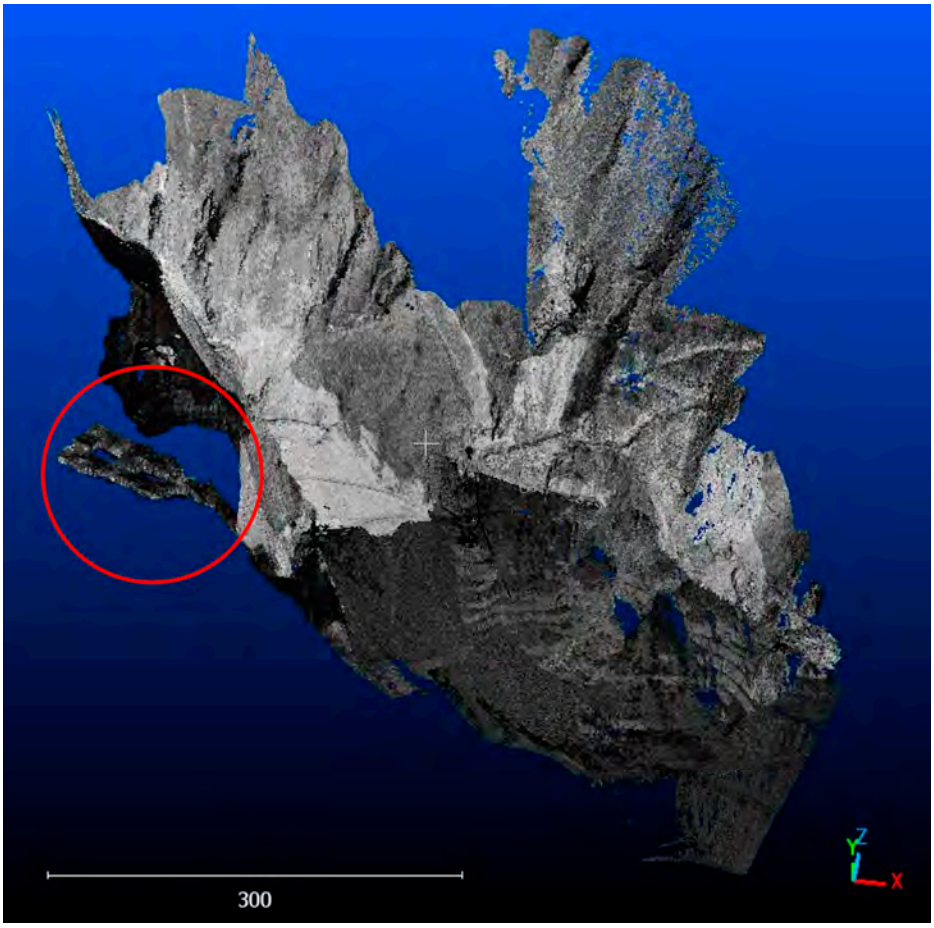

Figure 4. Three-dimensional point cloud of the open-pit quarry area and underground tunnel (highlighted by the red circle).

3.2. Geomechanical Characterization

Geomechanical characterization of marbles involves determining both the intact rock properties and the discontinuity pattern of the rock mass. The parameters of the intact rock were collected from several sources, including a technical report by the quarry property [29], the Catalogue of Commercial Varieties of Apuan Marbles [32], and relevant published studies [33,34]. In addition, during this study in situ biaxial compression tests were performed to directly measure the marble's elastic constants. These tests yielded site-

specific values for Young's modulus and Poisson's ratio, which are included among the intact rock properties summarized in Table 1.

Table 1. Intact rock geomechanical parameters.

Parameter	Value
Uniaxial Compressive Strength (MPa)	100
Tensile Strength (MPa)	8 ± 3
Cohesion (MPa)	20
Friction Angle (°)	50
Density (Kg/m^3)	2700
Poisson's coefficient (-)	0.35
Young's Modulus (MPa)	84,000

In parallel, the structural discontinuities within the rock mass were surveyed to characterize the fracture network. Relevant data on rock fractures were obtained from geological–structural surveys, aimed at evaluating the fracture density and characteristics in the quarry area. The surveys were conducted at key locations, including the area near the underground entrance, and along the base of the southwestern quarry faces (Figure 5). In total, about 300 discontinuity measurements were collected.

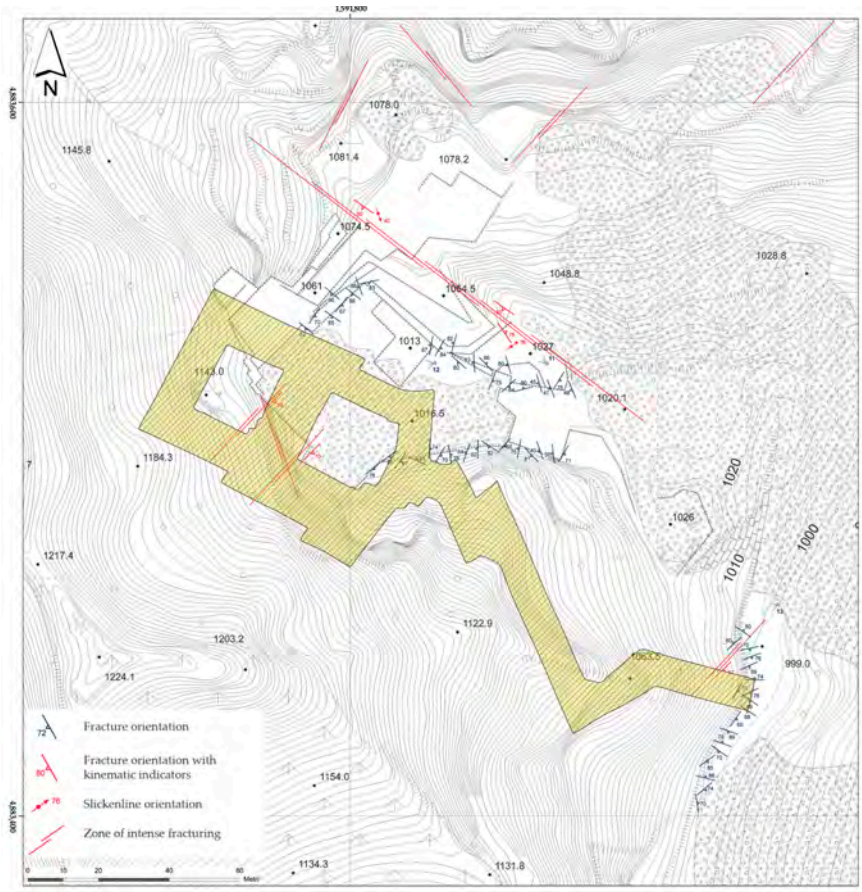

Figure 5. Extract from the map of discontinuities (modified from [29]). The yellow area indicates the underground tunnel.

3.3. CSIRO HI Cell Overcoring Tests

To evaluate the in situ stress state of the rock mass, a series of stress measurements were performed on the walls of the underground quarry. Four overcoring tests using the CSIRO HI cell method were carried out. These tests were conducted at different depths in two sub-horizontal boreholes that had been specifically drilled into the walls of the underground excavation (Figures 6 and 7). The overcoring measurements were done at depths ranging from 5.09 m to 10.34 m from the tunnel walls. Each of the four CSIRO HI tests provided a full three-dimensional stress tensor for the rock at the test location. Dip directions, dips, diameters, and depths of the boreholes and test points are summarized in Table 2.

Figure 6. Stages of a sub-horizontal borehole drilling.

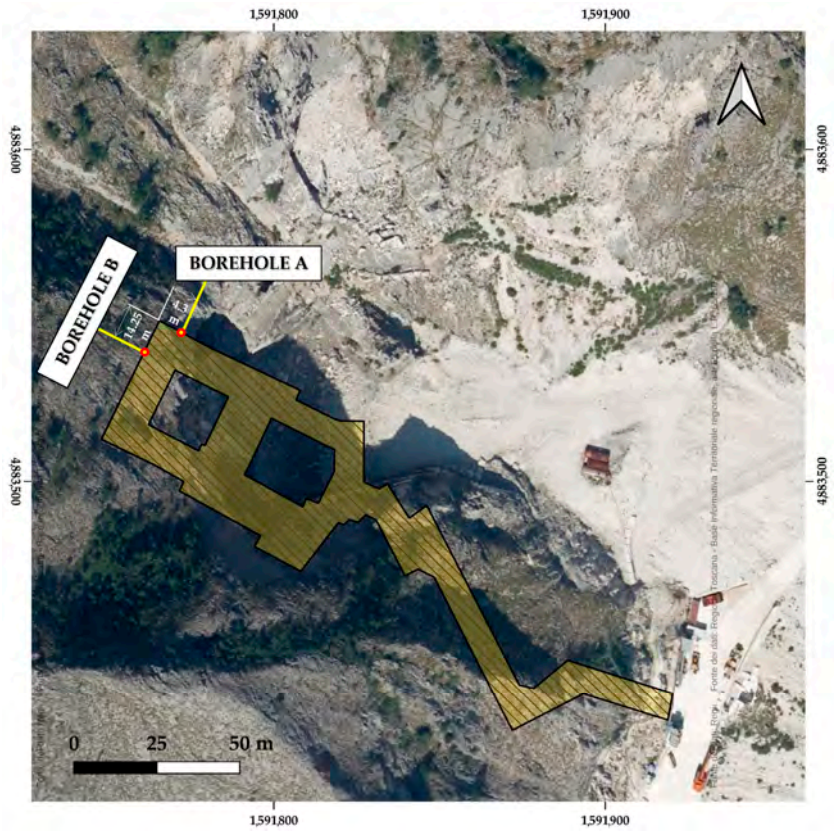

Figure 7. Orthophoto of the quarry area with the overlay of the underground tunnels (in yellow) and location of the executed CSIRO HI tests.

Table 2. Size, orientation, and depth characteristics of the boreholes.

Borehole	Bore Diameter (mm)	Dip Direction (°)	Dip (°)	Depth of the CSIRO HI Test (m)	
A	164	26	5	A1	5.65
				A2	10.65
B	164	296	5	B1	5.40
				B2	10.34

In addition to the overcoring measurements, complementary tests were performed to determine the rock's elastic behavior under load. Radial compression tests on core samples extracted from the site were conducted using a Hooke biaxial cell (Figure 8), providing independent measurements of the marble's elastic parameters (Young's modulus E, and Poisson's ratio ν).

Figure 8. Stages of biaxial compression testing using the Hooke biaxial cell at the Ravalunga quarry.

3.4. Distinct Element Numerical Modelling

The numerical analyses were performed using 3DEC v7 [8], a Distinct Element Method code that allows for the representation of fractured rock masses as deformable blocks separated by discontinuities [35]. The geometry of the Ravalunga quarry was built starting from high-resolution geomatic data: the external morphology (Figure 9) was reconstructed by combining data from a UAV photogrammetric survey with a regional 3D point cloud obtained from airborne LiDAR at 1 m of resolution. Figure 10 shows a detailed representation of the 3D model of the external surface built in mesh format by means of Agisoft Metashape™ v. 2.0.2 and Rhinoceros™ v. 8 software. Similarly, the underground tunnels were modelled as an internal cavity based on data from TLS (Figure 10). The extension of the numerical domain is approximately 850 × 600 × 550 m, and it is discretized into ~15,000 mesh faces.

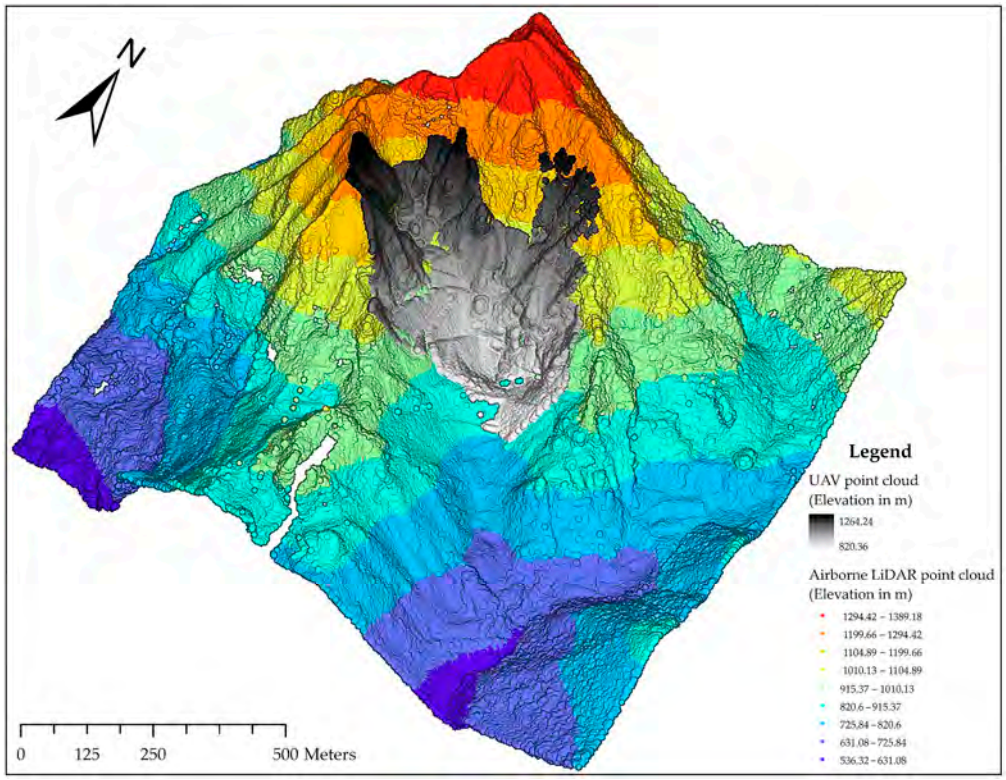

Figure 9. Three-dimensional point cloud of the external topographic surface. Gray points represent the drone-based photogrammetric survey, while colored points derive from airborne LiDAR data.

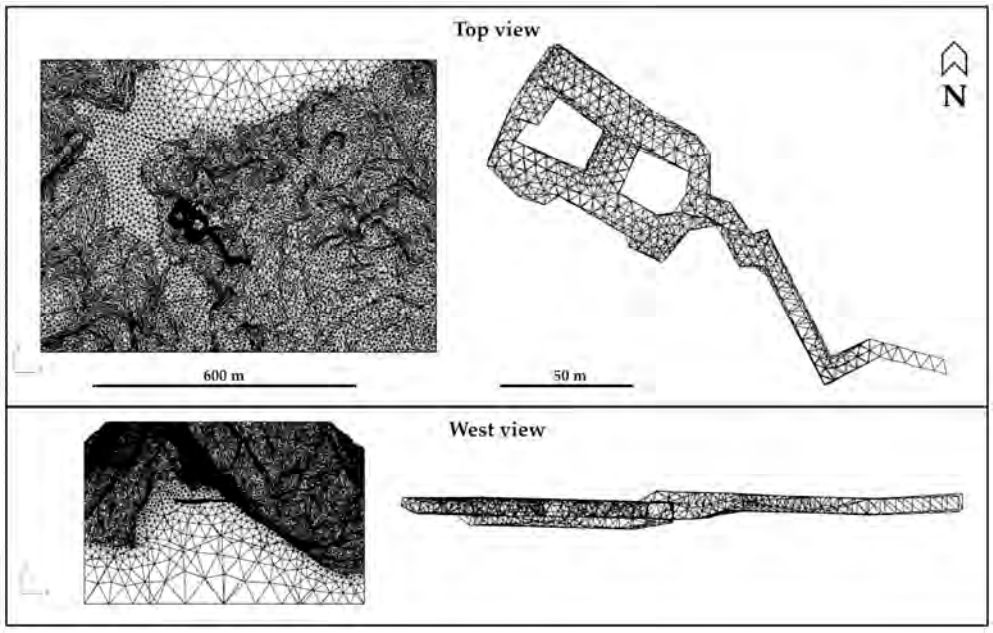

Figure 10. Mesh of the topographic surface used to build the quarry model. On the left the entire quarry model, on the right the underground tunnel in top and lateral west view.

The intact rock was represented by deformable blocks of elastic–perfectly plastic Mohr–Coulomb behavior [36]. Given that Carrara marble exhibits an almost purely elastic response up to peak strength [23], this constitutive model is suitable for representing the material behaviour under the pre-failure stress conditions considered in this study. Density, Young's modulus, Poisson's ratio, cohesion, and friction angle from laboratory and in situ tests were assigned to the material. The main joint sets were introduced as

planar discontinuities with their measured orientation, spacing and persistence and their mechanical behaviour was reproduced with a Coulomb slip law [37]; their mechanical properties were defined by the following parameters: cohesion (MPa), friction angle (°), and stiffness (Pa/m) in terms of normal (Kn) and shear (Ks) stiffness. These lasts were computed according to the Coulomb slip criterion [37].

Static boundary conditions included a fixed lower surface and lateral restraints, implemented by imposing zero velocity at the base and along the model sides. The topographic surface remained free and unconstrained.

After applying gravity, the model was initialized with the in situ stress field derived from CSIRO HI overcoring measurements. For each borehole, the principal stresses (i.e., σ_1, σ_2, σ_3), their orientations and magnitudes, together with the corresponding depth and spatial coordinates, were imported into the numerical model. The stress values were then assigned in 3DEC at the measured locations, incorporating lithostatic stress increase with depth to obtain a realistic stress gradient within the rock mass. This ensured that the numerical response was consistent with the real stress state of the rock mass as recorded at the precise locations.

Figure 11 shows the created three-dimensional model that was employed for numerical analysis, while Figure 12 represents a detail of the northeastern side of the underground entrance.

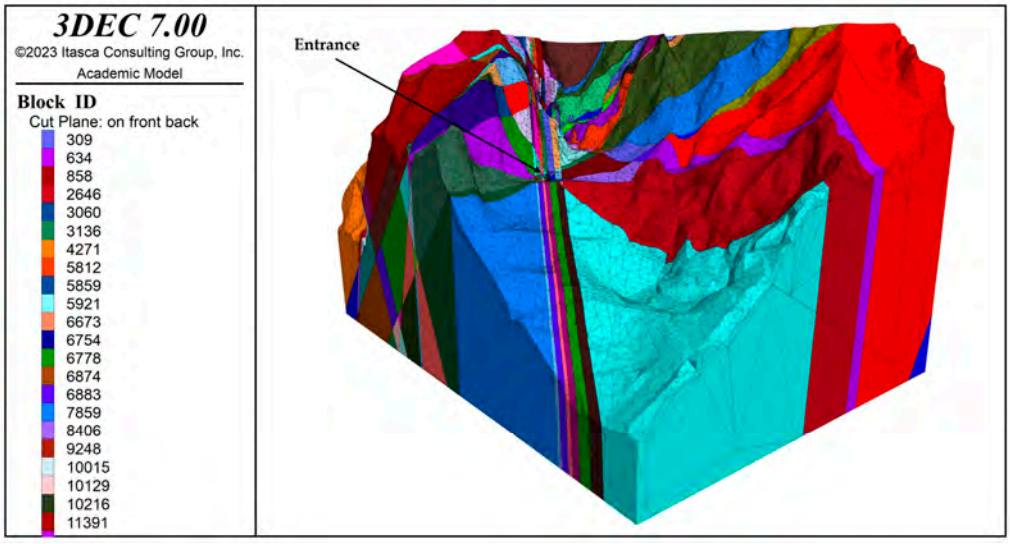

Figure 11. Three-dimensional model employed for numerical analysis in 3DEC v.7.

Afterwards, a dynamic analysis was performed using an explicit time-integration scheme, with quiet/absorbing lateral boundaries to minimize artificial wave reflections, while the seismic time-history was applied as a velocity input at the model base [38]. According to NTC 2018 [39] the adopted seismic loading corresponds to the Life Limit State of the Ravalunga site (namely Carrara) with Return Period (*Tr*) of 475 years. The input motion was defined as an horizontal base velocity time-history derived from the NTC 2018 response spectrum (ESSE1 parameters) for the site, with the following characteristics: reference peak ground acceleration *ag* equal to 0.168 g, spectral amplification factor F_0 equal to 2.398, and corner period *Tc* equal to 0.286 s (dominant frequency ≈ 3.5 Hz, used for Rayleigh damping calibration). The seismic signal was generated using the GeoStru online platform [40] from an NTC-based synthetic base accelerogram, with *ag* equal to 0.20 g, and subsequently scaled by a factor of 0.840 to match the site-specific hazard level. The resulting velocity-time history (.tab format) was imported into 3DEC as the X-base input motion. A light Rayleigh mechanical damping was introduced to reduce high-frequency

numerical noise while preserving the physically meaningful response [8,41]. The mass-proportional damping constant α was set equal to 0.05, while the stiffness-proportional damping constant β to 3.5. These constants were obtained using GeoStru seismic tool [40], which calculates the optimal damping values starting from the NTC 2018 design spectrum and its predominant frequency. The resulting parameters were then assigned in 3DEC to ensure consistency between the reference seismic input and the dynamic numerical model. The model response was evaluated by analyzing the stress and deformation fields within both the underground tunnels and the external quarry faces.

(**a**) (**b**)

Figure 12. Northeast perspective view of the underground tunnel entrance, as modelled in 3DEC v.7 (**a**) and photographed from the access road to the quarry (**b**).

4. Results

4.1. Engineering-Geological Survey

A statistical analysis of the discontinuities measured during engineering-geological survey allowed us to identify six principal joint sets, labeled K1, K2.1, K2.2, K3, K4, and K5. The average orientation and other physical characteristics of discontinuity sets (frequency, persistence and spacing) are summarized in Table 3.

Table 3. Discontinuity sets mapped at Ravalunga quarry.

Set	Dip Direction	Dip	Frequency %	Persistence (m)	Spacing (m)
K1	030	89	33	>20	0.6
K2.1	128	71	25	3–20	0.8
K2.2	296	72	7	1–10	1.2
K3	257	88	19	3–20	1.2
K4	165	87	10	1–3	1
K5	255	46	3.5	>20	1.2

4.2. CSIRO HI Stress Measurements

Four CSIRO HI overcoring tests (A1–A2 and B1–B2) were completed within the underground excavation at depths variable between ~5 and ~10 m beyond the wall surface. Overcoring and biaxial compression tests were permitted to derive the full 3D stress tensor together with elastic parameters of the marble at the test location. A concise summary of the computed data is provided in Table 4.

Table 4. Results from CSIRO HI tests (± indicates 68% confidence limits). Abbreviations: E—Young's modulus, ν—Poisson's ratio; σ_1, σ_2, σ_3—maximum, intermediate, and minimum principal stresses (+ sign indicates compression); σ_v—vertical component of the stress tensor (+ sign indicates compression).

Borehole	Depth (m)		E [MPa]	ν [-]	σ_1 [MPa]	σ_2 [MPa]	σ_3 [MPa]	σ_v [MPa]
A	A1	5.65	82,797 ± 1036	0.36 ± 0.02	13.35 ± 0.48	3.74 ± 0.36	2.76 ± 0.65	10.74 ± 0.39
	A2	10.65	81,742 ± 1690	0.35 ± 0.03	7.90 ± 0.23	3.88 ± 0.15	2.57 ± 0.28	6.79 ± 0.14
B	B1	5.40	87,572 ± 1654	0.33 ± 0.02	9.26 ± 0.28	2.20 ± 0.38	0.04 ± 0.21	8.15 ± 0.22
	B2	10.34	84,749 ± 1785	0.32 ± 0.03	5.03 ± 0.31	2.38 ± 0.47	0.22 ± 0.30	4.55 ± 0.39

4.3. DEM Modelling

Under static conditions, the three-dimensional numerical model of the Ravalunga quarry was first brought to static equilibrium under gravity using an initial stress field calibrated from CSIRO HI measurements and mechanical properties for intact rock (Table 5) and joints (Table 6). The analysis focused on the distribution of displacements and maximum shear stresses (τ_{max}), as these parameters represent the main markers of deformation and potential shear activation within a fractured marble rock-mass.

Table 5. Summary of the mechanical parameters assigned to the intact rock used in the construction of the numerical model. Abbreviations: Ei—Young's modulus of intact rock, ν—Poisson's ratio; Gi—Shear modulus of intact rock.

Friction Angle (°)	Cohesion [MPa]	Density [kg/m^3]	Ei [MPa]	ν [-]	Gi [MPa]
50	20	2700	84,000	0.35	31,111

Table 6. Mechanical parameters of the rock mass and discontinuities adopted in the numerical model. Abbreviations: Em—Young's modulus of the rock mass; Gm—Shear modulus of the rock mass; L—verage joint spacing; Kn—joint normal stiffness; Ks—joint shear stiffness.

Friction Angle (°)	Em [MPa]	Gm [MPa]	L [m]	Kn [MPa/m]	Ks [MPa/m]
35	58,023	21,490	1	187,624	69,491

Results are presented both at the scale of the entire quarry and, more in detail, for the underground tunnels. To focus interpretation on the working area, a horizontal section, named AA′ in Figure 13 and passing through the drill point of borehole A, was extracted.

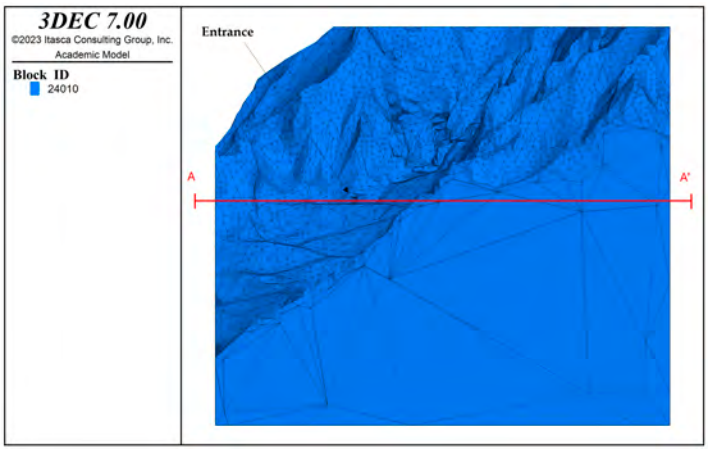

Figure 13. Lateral westward view of the 3D model with the horizontal section AA′ represented in red.

The computed displacement field shows generally low magnitudes throughout the quarry domain with highest values reaching at most 4–7 mm (Figure 14). Within the underground excavation (Figure 15), the deformation field remains uniform, with displacements ranging between 3 and 6 mm, indicating negligible differential movement and limited kinematic response.

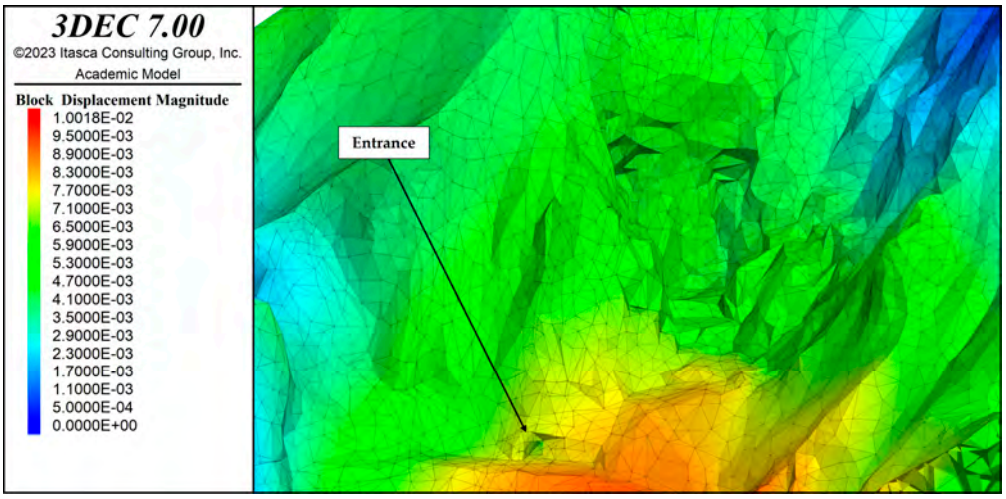

Figure 14. Distribution of displacements in the static simulation.

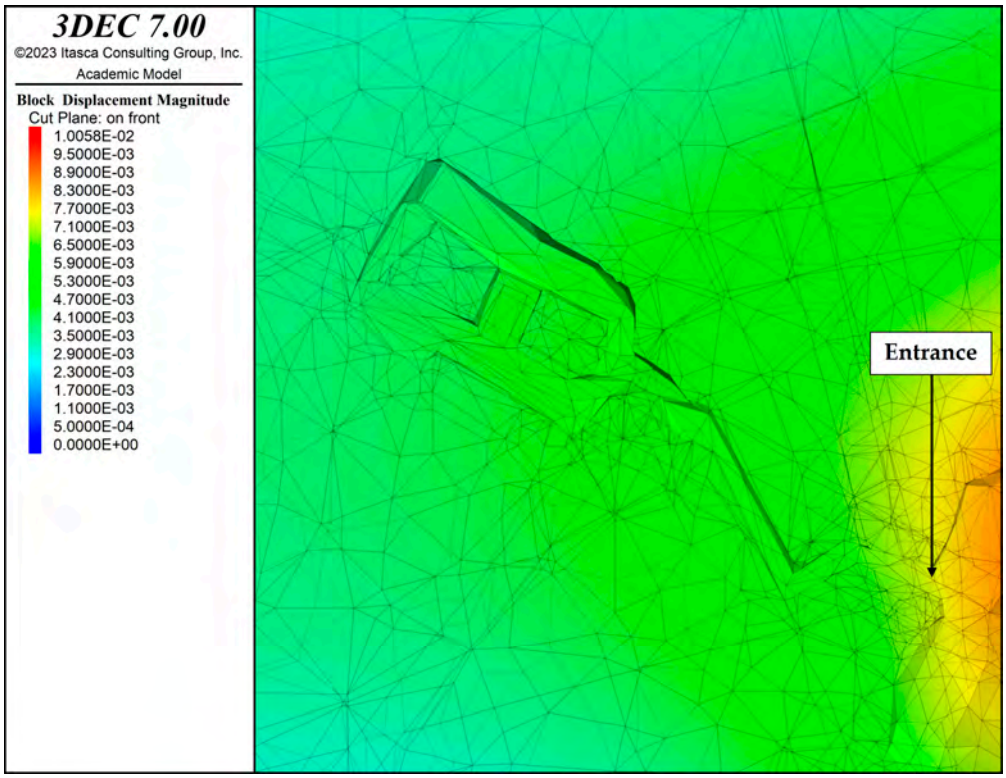

Figure 15. Horizontal section (AA′) of the underground excavation, showing the distribution of displacement values in the static simulation.

The distribution of maximum shear stress (τ_{max}) in the whole quarry area rarely exceeds 7 MPa (Figure 16), while inside the tunnel it varies between 2 and 10 MPa. The highest values, typically between 7 and 10 MPa, are concentrated at pillar corners, roof–wall junctions, and around the portal (Figure 17).

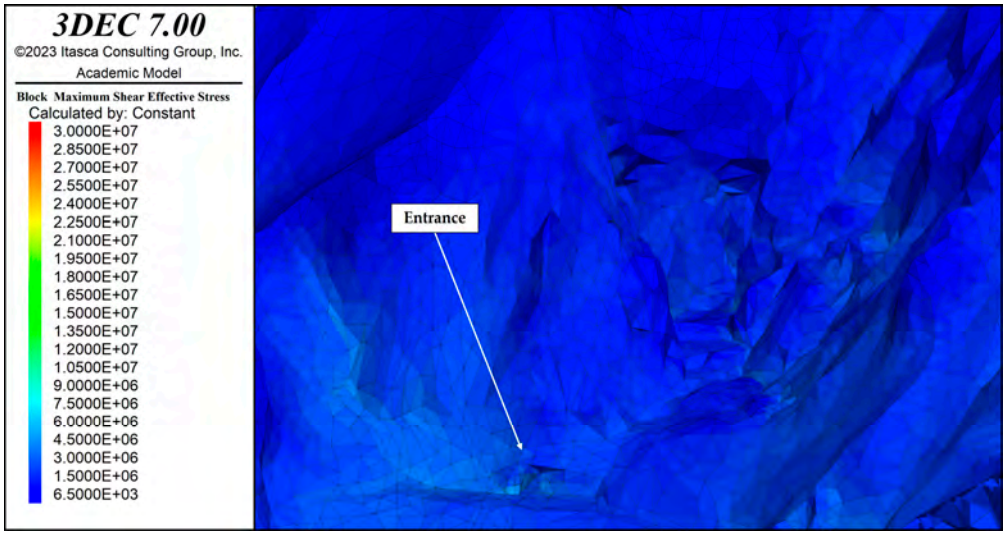

Figure 16. Distribution of maximum shear stress values (τ_{max}) in the static simulation.

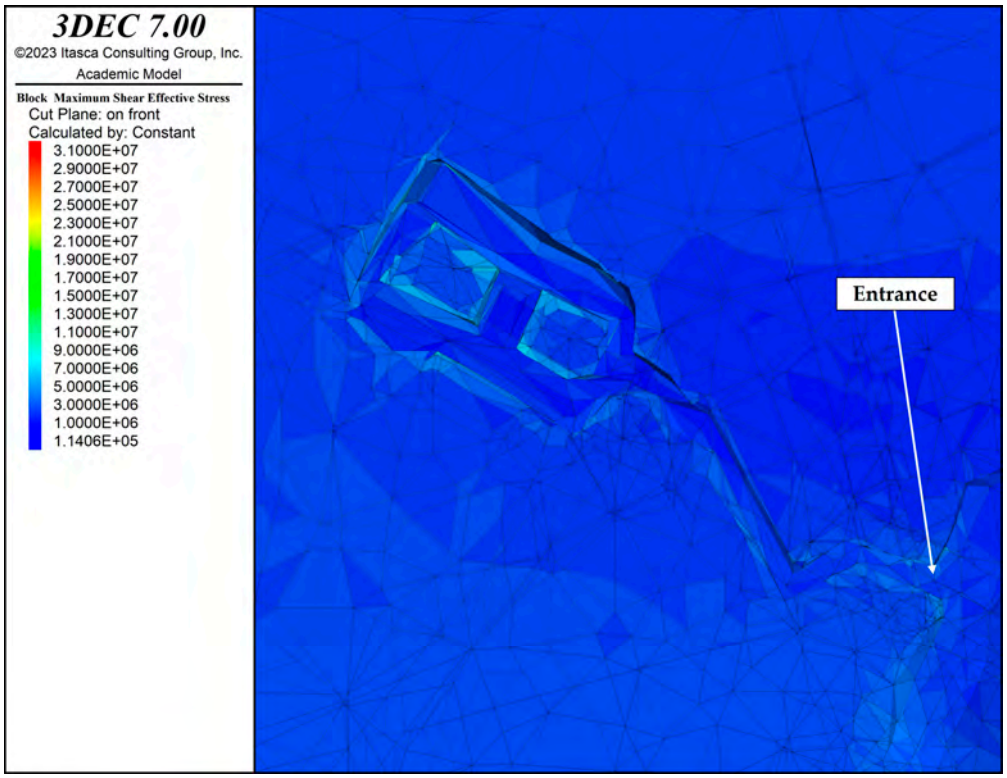

Figure 17. Horizontal section (AA′) of the underground excavation, showing the distribution of maximum shear stress values (τ_{max}) in the static simulation.

Dynamic simulations were lately performed by applying a base-input horizontal motion consistent with the NTC 2018 [39] design spectrum, obtained from the GeoStru national database [40] and converted into a velocity-time history file to be used in 3DEC.

The displacement field under dynamic conditions displays a pattern broadly similar to that observed in the static case with values ranging from 3 to 5 mm both for the external quarry slopes (Figure 18) and the underground domain (Figure 19). Some exceptions, with highest displacement gradients up to decimeters, are present at the open-pit excavation walls of the inactive quarry where free surfaces intersect unfavorably oriented discontinuities, producing potential sliding interfaces for small surface blocks (Figure 20).

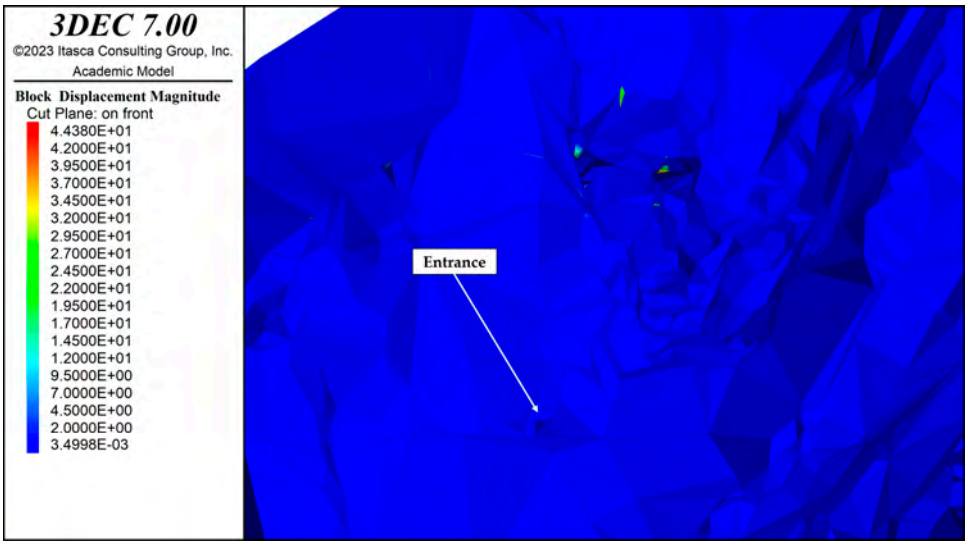

Figure 18. Distribution of displacement values in the dynamic simulation.

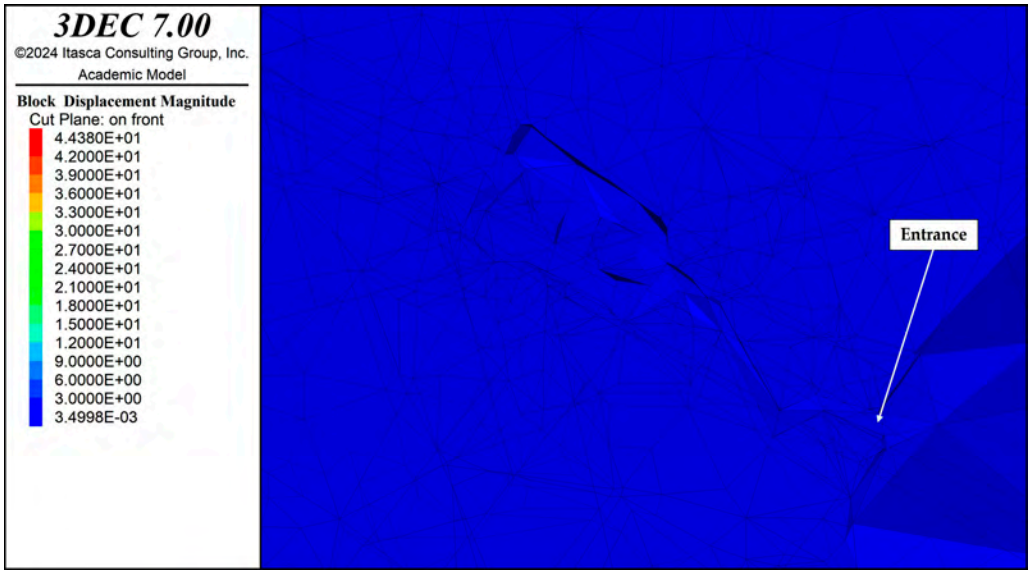

Figure 19. Horizontal section (AA′) of the underground excavation, showing the distribution of displacement values in the dynamic simulation.

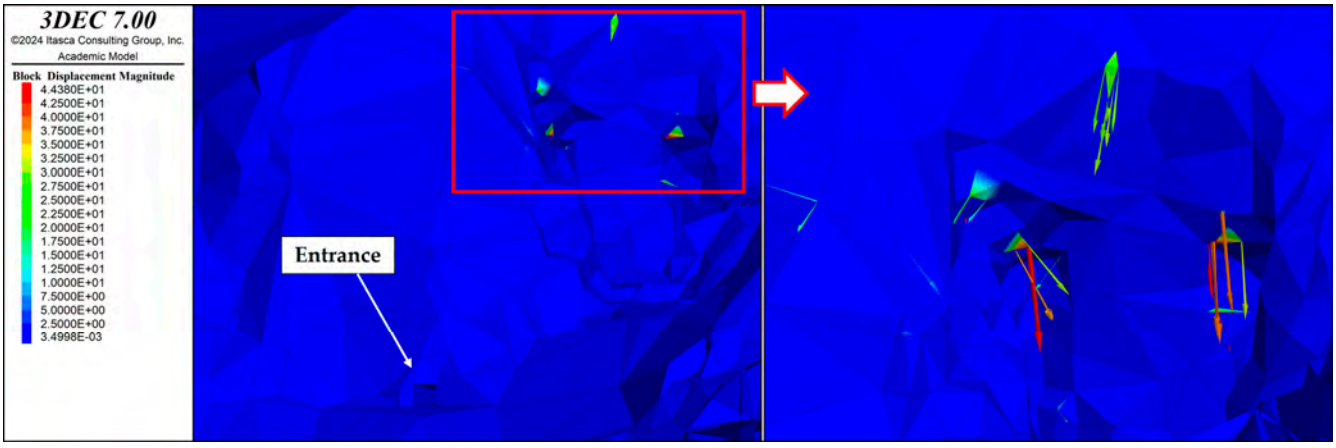

Figure 20. Potential sliding interfaces for small surface blocks and relative displacement vectors.

The evolution of maximum shear stress (τ_{max}) during seismic excitation generally mirrors the static distribution with peak values within the same range between 6–10 MPa (Figure 21). However, localized dynamic amplifications are recorded both along the walls of the inactive open-pit quarry and at geometric intersection of discontinuities within the underground excavation (Figure 22). In particular, peaks of τ_{max} exceeding 20 MPa occur at sharp excavation corners (e.g., pillar edges, roof–wall junctions) and where fracture planes intersect free surfaces.

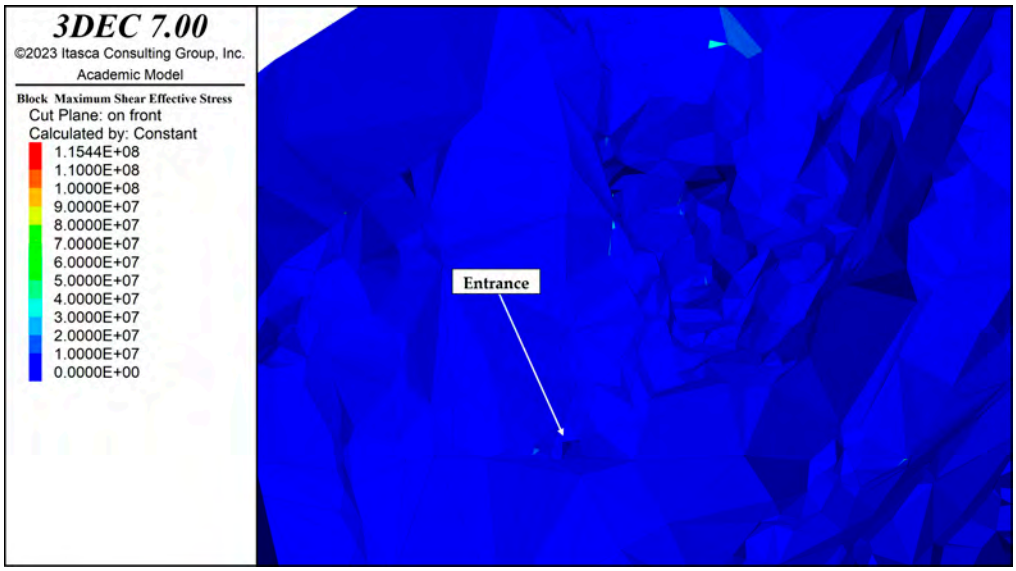

Figure 21. Distribution of maximum shear stress values (τ_{max}) in the dynamic simulation.

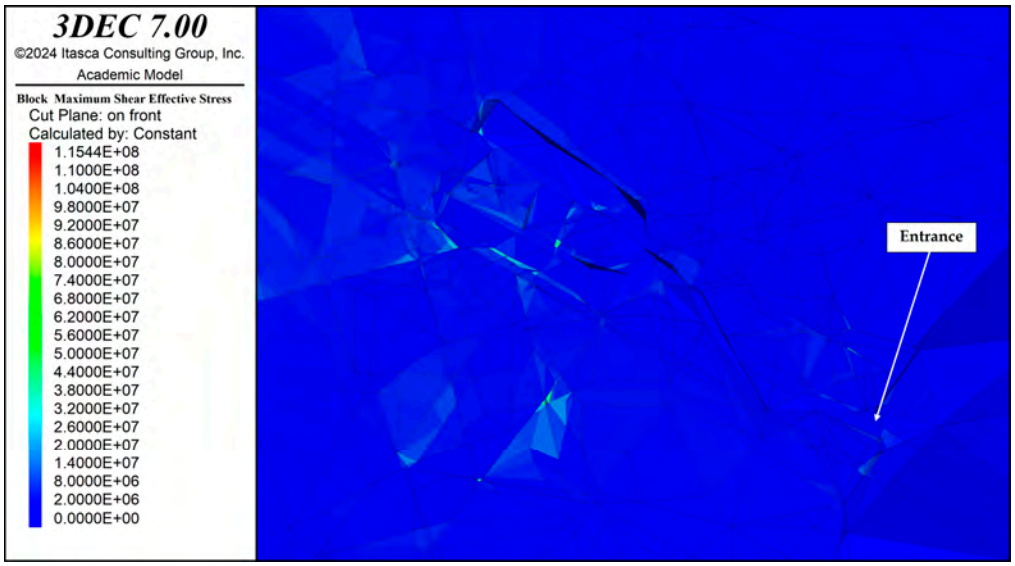

Figure 22. Horizontal section (AA′) of the underground excavation, showing the distribution of maximum shear stress values (τ_{max}) in the dynamic simulation.

5. Discussion

The physically calibrated DEM model—built on high-resolution survey geometry and initialized with in situ stress tensors from CSIRO HI testing—enabled a reliable interpretation of both static and dynamic stability conditions at the Ravalunga marble quarry. The behavior of the rock mass, as resulting from the simulations, is characterized by high stiffness and strong confinement, consistent with what is typically observed in massive carbonate formations [42].

In fact, under static conditions, the numerical modeling shows peak values of shear stresses of approximately 10 MPa and displacements of 4–7 mm. These modest values are consistent with a high elastic modulus material.

Highest values of stress are mainly concentrated at sharp geometric features, such as pillar corners and wall–roof intersections. This reflects well-known mechanisms of stress redistribution in fractured rock masses where excavation geometry plays a dominant structural role [42]. Despite these localized stress raisers, no significant yielding or progressive damage develop either within the underground chambers or along the external quarry faces, indicating an overall stable static configuration.

To assess if the maximum shear stress values obtained from the modelling are below the critical thresholds for the stability of the rock mass, the recorded values of maximum σ_1 and minimum σ_3 stress were used. According to Mohr's relation [43] the maximum shear stress τ_{max} corresponds to the semi-difference between the principal stresses σ_1 and σ_3, i.e.:

$$\tau_{max} = (\sigma_1 - \sigma_3)/2 \quad (1)$$

The difference between $\sigma_1 - \sigma_3$ is named "deviatoric stress" (τ_d) and it can be calculated with the following formula:

$$\tau_d = 2\tau_{max} \quad (2)$$

In this case study, the maximum shear stress τ_{max} at the current excavation stage is about 10 MPa; hence, the deviatoric stress ($\sigma_1 - \sigma_3$) is equal to 20 MPa.

To critically evaluate the sustainability of the deviatoric stress values obtained during numerical modelling, the generalized Hoek and Brown criterion [4] can be used according to the following equation:

$$\sigma_1 = \sigma_3 + \sigma_{ci}(m_b \frac{\sigma_3}{\sigma_{ci}} + s)^a \quad (3)$$

where σ_{ci} denotes the intact rock uniaxial compressive strength (100 MPa in this case study—see Table 1) and m_b and s are empirical constants.

Referring to [44], a fractured rock mass undergoes new fractures when the deviatoric stress $\sigma_1 - \sigma_3$ exceeds the Hoek & Brown criterion [4] formulated with mb = 0 and s = 0.11. In this case, the failure criterion [4] becomes:

$$\sigma_1 - \sigma_3 \approx 0.33\ \sigma_{ci} \quad (4)$$

Considering the value of uniaxial compressive strength equal to 100 MPa, it follows that the rock mass of the Ravalunga quarry may exhibit critical conditions only in areas where the deviatoric stress exceeds the threshold of $\sim$ 33 MPa. Been the maximum deviatoric stress value obtained from modelling, in static simulation, equal to $\sim$ 20 MPa, it follows that τd of the Ravalunga quarry is below the calculated threshold.

As a stricter material-specific check, the results can also be evaluated according to the deviatoric stress limit proposed for Carrara Marble by [45], calculated as follows:

$$\sigma_1 - \sigma_3 \gtrsim 0.20\ \sigma_{ci} \quad (5)$$

In this case the threshold for the deviatoric stress become $\sim$ 20 MPa (equal to the maximum deviatoric stress value obtained from modelling). The computed deviatoric stress reaches—but does not exceed—this conservative limit for Carrara marble and, more than a critical state in absence of instability indicators, must be interpreted as a warning threshold for the current geometry and loading conditions.

In contrast, a different response emerges under seismic loading where localized dynamic effects arise in correspondence of free faces and geometric discontinuities. In particular, τ_{max} spikes exceeding 20 MPa were observed at internal pillar corners, mainly

where joint planes intersect excavation boundaries, thus exceeding the proposed thresholds. These peaks are localized and spatially restricted and could be explained by three concurrent mechanisms:

- Geometric amplification at sharp excavation corners, acting as stress concentrators [46,47];
- Constructive interference of wave fronts at free surfaces, enhancing dynamic shear stress [48];
- Favorably oriented fractures that locally reduce shear stiffness and promote stress transfer [49,50].

Anyhow, it must be emphasized that the ongoing excavation activity already includes the installation of active protection works, primarily rock bolts and steel sets/arches (Figure 23). While their presence has not been included in the current numerical modeling due to a lack of information on their dimensions, characteristics, and force, it is undoubtedly a positive factor to be considered.

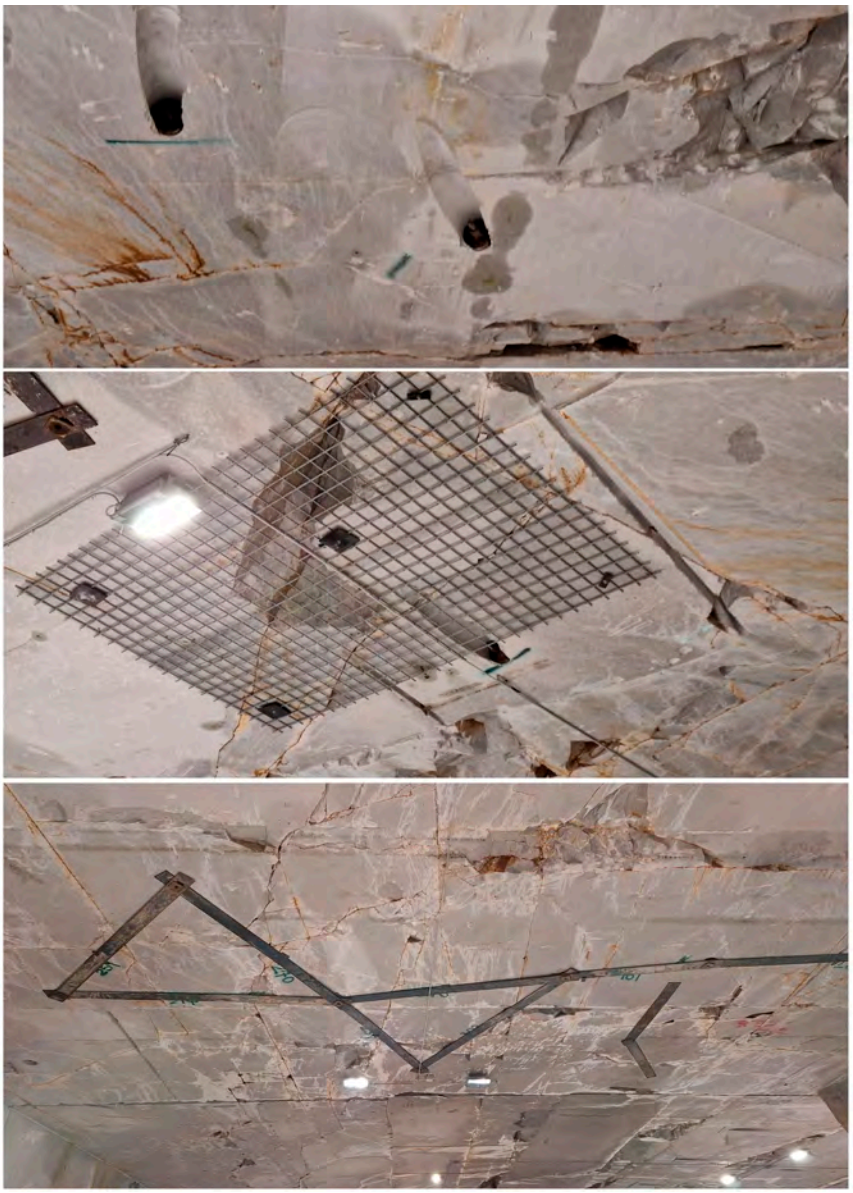

Figure 23. Examples of active supports installed in the roof of the underground tunnels.

Some criticalities are observed also along the free surfaces of the open-pit quarry. The lack of confinement combined with fractures unfavorably oriented with respect to the excavation fronts results in considerable dynamic displacements. In these areas, seismic loading may lead to temporary mobilization of shallow surface blocks—a mechanism consistent with the discontinuous nature of the rock mass [51] as shown in Figure 20. These mobilizations are due to topographic amplification and are limited to the free surface without involving deeper or structurally important rock volumes [52]. These criticalities highlight the need for targeted operational improvements in specific areas of the quarry. Dynamic displacements observed along open-pit free surfaces suggest priority zones where (i) optical monitoring systems and (ii) controlled removal or reinforcement of shallow unstable blocks should be implemented. In addition, the τ_{max} concentrations exceeding 20 MPa at internal pillar corners identify areas where (iii) localized bolting or anchor reinforcement is most appropriate. In addition, (iv) extensometers should be installed on joints that exhibited preferential displacement vectors during dynamic loading, while (v) microseismic or acoustic emission monitoring may be employed to detect precursory slip along fractures characterized by unfavorable orientations.

Noticeably, any advancement in the quarry shape and modification of the structural setting must be included in the routine updates since every change can alter the model response.

The comparison between static and dynamic conditions highlights the crucial role of realistic stress initialization. Using CSIRO HI measurements ensures that modeled stress paths reflect the actual in situ state rather than oversimplified lithostatic assumptions, improving the predictive reliability of DEM simulations [19,27,28,53]. In fact, the physically calibrated model successfully identifies the most vulnerable zones of the rock mass. The distinguishing contribution of this work lies in demonstrating that coupling direct in situ stress measurements with DEM simulation in a physically constrained workflow—both in static and dynamic condition— significantly supports the reliability of local predictions and provides a sound, field-validated basis for engineering decisions.

6. Conclusions

This study demonstrates that integrating a 3D DEM numerical model with high-resolution geomatic data, detailed structural characterization, and direct in situ stress measurements (by CSIRO HI cell tests) provides a calibrated and site-specific assessment of stability for the Ravalunga quarry. Under static conditions, the marble rock mass exhibits the expected behaviour of a stiff and well-confined material: displacements remain at the millimetric scale, and maximum shear stresses are below critical thresholds, both according to the Hoek–Brown criterion [4] and to conservative values proposed for Carrara marble by Gullì et al. [45].

Dynamic analysis conducted using seismic input consistent with the NTC 2018 spectrum [39], confirms the substantial stability of the underground tunnels, although localized and short-lived peaks of maximum shear stress exceeding the proposed threshold (i.e., 20 MPa) may occur at sharp geometric corners of internal pillars and at free surfaces. These peaks are attributed to the combined effect of geometric stress amplification, wave reflection at free boundaries, and fracture orientations that efficiently transmit shear motion during shaking. Despite these transient stress concentrations, no progressive damage or loss of confinement develop within the tunnel, indicating stable behavior under the applied seismic scenario. Furthermore, the current quarry context already includes active protective structures, not yet modeled due to a lack of information on their characteristics, but which play a positive role in terms of wall stability.

Potential instability is instead concentrated at external quarry faces, where reduced confinement and unfavourable joint orientations can facilitate the temporary mobilization of shallow blocks during seismic excitation. These processes remain limited to near-surface volumes and do not involve deeper, structurally significant rock masses and can be solved or monitored by maintenance actions widely used in mining activity. Localized bolting or anchoring of exposed blocks identified as vulnerable by the model, together with periodic UAV/TLS surveys and focused visual inspections could be adopted to detect early displacement signals.

The main contribution of this work lies in demonstrating that the integration of direct stress measurements into DEM modelling substantially improves confidence in stability predictions and supports engineering decisions grounded in physical evidence. This approach represents a concrete step toward safer and more sustainable management practices for fractured marble quarries. Another key finding of this study is that only the dynamic analysis is able to capture all potential instability mechanisms: certain critical conditions emerge only under seismic loading, when reduced confinement and joint kinematics become significant. Therefore, an integrated assessment of both static conditions and dynamic response is essential to ensure a fully reliable evaluation of stability in fractured rock quarry environments. Looking ahead, future development could include validation through field monitoring to compare real deformations and possible failures with model predictions and further consolidate the reliability of the proposed approach.

Author Contributions: R.S. was the Project Coordinator for the University of Siena; R.S. was involved in the review and supervision of the study. D.G. and D.M. coordinated research activities on behalf of the UOC Ingegneria Mineraria—USL Toscana Nord-Ovest, Tuscany Region; V.D.L. and R.S. carried out surveys and contributed writing and editing to this manuscript. V.D.L. contributed to the analysis, processing, validation, and care of the data. V.D.L. performed 3D modelling and rock slope stability analysis using 3DEC© v7. All authors have read and agreed to the published version of the manuscript.

Funding: This research was funded by Tuscany Region through the UOC Ingegneria Mineraria—USL Toscana Nord-Ovest.

Institutional Review Board Statement: Not applicable.

Informed Consent Statement: Not applicable.

Data Availability Statement: The original contributions presented in this study are included in the article. Further inquiries can be directed to the corresponding authors.

Acknowledgments: We would like to thank the quarry property for providing all the available data and technical reports, and for allowing us to publish it alongside this study.

Conflicts of Interest: The authors declare no conflicts of interest.

References

1. Santa, C.M.; Fernandes, I.; Chaminé, H.I. Geomechanical Classifications, Geotechnical Indexes and Fractured Rock Media: The Influence of Discontinuities on the Rock Masses Description. *Civ. Environ. Eng. Rep.* **2024**, *3*, 43–54. [CrossRef]
2. Barton, N.R. A model study of rock-joint deformation. *Int. J. Rock Mech. Min. Sci. Geomech. Abstr.* **1972**, *9*, 579–582. [CrossRef]
3. Gottron, D.; Henk, A. Upscaling the Mechanical Properties of a Fractured Rock Mass Using the Lattice-Spring-Based Synthetic Rock Mass (LS-SRM) Modeling Approach—Comparison of Discontinuum, Continuum and Empirical Approaches. *Geosciences* **2022**, *12*, 343. [CrossRef]
4. Hoek, E.; Brown, E.T. The Hoek–Brown failure criterion—A 2018 update. *J. Rock Mech. Geotech. Eng.* **2019**, *11*, 585–592. [CrossRef]
5. Brady, B.H.G.; Brown, E.T. *Rock Mechanics for Underground Mining*, 3rd ed.; Springer: Dordrecht, The Netherlands, 2006; pp. 1–600.
6. Wang, T.; Xu, D.; Elsworth, D.; Zhou, W. Distinct element modeling of strength variation in jointed rock masses under uniaxial compression. *Geomech. Geophys. Geo-Energy Geo-Resour.* **2016**, *2*, 11–24. [CrossRef]

7. An, H.; Wu, S.; Liu, H.; Wang, X. Hybrid Finite-Discrete Element Modelling of Various Rock Fracture Types. *Sustainability* **2022**, *14*, 592. [CrossRef]
8. Itasca Consulting Group, Inc. *3DEC, 3-Dimensional Distinct Element Code User's Guide*; Itasca Consulting Group, Inc.: Minneapolis, MN, USA, 2024. Available online: https://www.itascacg.com/3dec (accessed on 10 October 2025).
9. Ge, X.; Liu, X. Effects of Three-Directional Seismic Wave on Dynamic Response and Failure Behavior of High-Steep Rock Slide. *Appl. Sci.* **2022**, *12*, 20. [CrossRef]
10. Zhou, Y.; Zhao, Z.; Li, H.; Liu, D. DEM-Based Numerical Investigation of Seismic Stability of Jointed Rock Masses Using 3DEC. *Lithosphere* **2021**, *2021*, 613345. [CrossRef]
11. Ziegler, M.O.; Heidbach, O. The 3D Stress State from Geomechanical–Numerical Modelling: Quantification of Uncertainties in Stress Tensor Components. *Geotherm. Energy* **2020**, *8*, 33. [CrossRef]
12. Amadei, B.; Stephansson, O. *Rock Stress and Its Measurement*; Chapman and Hall: London, UK, 1997.
13. Ziegler, M.O.; Heidbach, O. Rock Properties and Modelled Stress State Uncertainties. *Rock Mech. Rock Eng.* **2022**, *55*, 2753–2774. [CrossRef]
14. Brown, E.T.; Hoek, E. Trends in relationships between measured rock stress and depth. *Int. J. Rock Mech. Min. Sci. Geomech. Abstr.* **1978**, *15*, 211–215. [CrossRef]
15. Hoek, E. *Practical Rock Engineering*; Rocscience: Toronto, ON, Canada, 2000.
16. Ferrero, A.M.; Migliazza, M.; Segalini, A.; Gullì, D. In situ stress measurements interpretations in large underground marble quarry by 3D modeling. *Int. J. Rock Mech. Min. Sci.* **2013**, *60*, 103–113. [CrossRef]
17. Bonetto, S.M.R.; Vagnon, F.; Umili, G.; Vianello, D.; Migliazza, M.R.; Ferrero, A.M. The Contribution of Remotely Sensed Data to the Stress State Evaluation in Underground Marble Quarries. *Egypt. J. Remote Sens. Space Sci.* **2021**, *24*, 1–13. [CrossRef]
18. Smith, W.K. *Two BASIC Computer Programs for the Determination of In Situ Stresses Using the CSIRO Hollow Inclusion Stress Cell and the USBM Borehole Deformation Gage*; USGS Open-File Report 82-489; U.S. Geological Survey: Reston, VA, USA, 1982. [CrossRef]
19. Jin, Z.; Li, Y.; Li, Q.; Liu, Z.; Wu, S.; Wang, Z. Modification of the CSIRO Method in the Long-Term Monitoring of Slope-Induced Stress. *Front. Earth Sci.* **2022**, *10*, 981470. [CrossRef]
20. De Lucia, V.; Ermini, A.; Guido, S.; Marchetti, D.; Gullì, D.; Salvini, R. Investigations using CSIRO HI Triaxial Cells for measuring the stress states of rock masses subject to mining extraction: Numerical modelling of in-situ extracted core samples. *Ital. J. Eng. Geol. Environ.* **2024**, *1*, 95–103. [CrossRef]
21. Pinheiro, A.L.; Lana, M.S.; Sobreira, F.G. Use of the Distinct Element Method to Study Flexural Toppling at the Pico Mine, Brazil. *Bull. Eng. Geol. Environ.* **2015**, *74*, 1177–1186. [CrossRef]
22. Stephansson, O.; Zang, A. ISRM Suggested Methods for Rock Stress Estimation—Part 5: Establishing a Model for the In Situ Stress at a Given Site. *Rock Mech. Rock Eng.* **2012**, *45*, 955–969. [CrossRef]
23. Gullì, D.; Pellegri, M.; Cortopassi, A. Experimental approach for stability evaluations of Carrara marble basins. In *Landslide Science and Practice, Vol. 3: Spatial Analysis and Modelling*; Springer: Berlin/Heidelberg, Germany, 2013; pp. 211–217.
24. He, M.; Jia, X.; Coli, M.; Livi, E.; Sousa, L. Experimental Study of Rockbursts in Underground Quarrying of Carrara Marble. *Int. J. Rock Mech. Min. Sci.* **2012**, *52*, 1–8. [CrossRef]
25. Francioni, M.; Salvini, R.; Stead, D.; Giovannini, R.; Riccucci, S.; Vanneschi, C.; Gullì, D. An Integrated Remote Sensing–GIS Approach for the Analysis of an Open Pit in the Carrara Marble District, Italy: Slope Stability Assessment through Kinematic and Numerical Methods. *Comput. Geotech.* **2015**, *67*, 46–63. [CrossRef]
26. Coli, M.; Criscuolo, A. The Carrara Marble: Geology, Geomechanics and Quarrying. *IOP Conf. Ser. Earth Environ. Sci.* **2021**, *833*, 012120. [CrossRef]
27. Salvini, R.; Ermini, A.; De Lucia, V.; Beltramone, L.; Silvestri, D.; Rindinella, A.; Guido, S.; Marchetti, D.; Gullì, D. Stress–strain investigation of the rock mass based on overcoring with CSIRO HI cell test and numerical modeling: A case study from an Italian underground marble quarry. *Geosciences* **2022**, *12*, 441. [CrossRef]
28. De Lucia, V.; Ermini, A.; Guido, S.; Marchetti, D.; Gullì, D.; Salvini, R. Distinct Element Numerical Modelling and In Situ CSIRO HI Cell Data for Rock Slope Stability Assessment. *Geosciences* **2025**, *15*, 155. [CrossRef]
29. Cortopassi, M.; Vaselli, O. *Piano di Coltivazione della Cava Ravalunga n.138 (Bacino di Colonnata—Loc. Ravalunga)*; Technical Report (Private Communication); Comune di Carrara: Carrara, Italy, 2013.
30. Cortopassi, P.F.; Daddi, M.; D'Amato Avanzi, G.; Giannecchini, R.; Lattanzi, G.; Merlini, A.; Milano, P.F. Quarry Waste and Slope Instability: Preliminary Assessment of Some Controlling Factors in the Carrara Marble Basin (Italy). *Ital. J. Eng. Geol. Environ.* **2008**, 99–118. [CrossRef]
31. Carmignani, L.; Kligfield, R. Crustal extension in the Northern Apennines: The transition from compression to extension in the Alpi Apuane core complex. *Tectonics* **1990**, *9*, 1275–1303. [CrossRef]
32. ERTAG Regione Toscana. *I Marmi Apuani*; Nuova Grafica Fiorentina: Florence, Italy, 1980; p. 126.
33. Cravero, M.; Gullì, D.; Iabichino, G. Comparative mechanical characterization of marble by means of laboratory testing. In Proceedings of the 39th U.S. Rock Mechanics Symposium (USRMS), Cambridge, MA, USA, January 2003.

34. Firpo, G.; Salvini, R.; Francioni, M.; Ranjith, P.G. Use of Digital Terrestrial Photogrammetry in rocky slope stability analysis by Distinct Elements Numerical Methods. *Int. J. Rock Mech. Min. Sci.* **2011**, *48*, 1045–1054. [CrossRef]
35. Cundall, P.A. The Measurement and Analysis of Acceleration in Rock Slopes. Ph.D. Thesis, University of London, London, UK, 1971.
36. Coulomb, C.A. Essai sur une application des règles des maximis et minimis à quelques problèmes de statique relatifs à l'architecture. *Mem. Acad. R. Sci.* **1776**, *7*, 343–387.
37. Jiao, Y.; Zhao, J.; Ge, X. New formulation and validation of the three-dimensional extension of a static relaxation method. *Adv. Eng. Softw.* **2004**, *35*, 317–323. [CrossRef]
38. Lysmer, J.; Kuhlemeyer, R.L. Finite dynamic model for infinite media. *J. Eng. Mech. Div.* **1969**, *95*, 859–877. [CrossRef]
39. Ministero delle Infrastrutture e dei Trasporti. *Decreto Ministeriale 17/01/2018. Aggiornamento delle "Norme Tecniche per le Costruzioni" (NTC 2018)*; Supplemento Ordinario alla Gazzetta Ufficiale n. 42 del 20 febbraio; Ministero delle Infrastrutture e dei Trasporti: Roma, Italy, 2018.
40. GeoStru Software. *GeoStru Online Platform—NTC 2018 Response Spectra and Seismic Input Generator*; GeoStru Software: Piacenza, Italy, 2024; Available online: https://www.geostru.eu (accessed on 6 November 2025).
41. Chopra, A.K. *Dynamics of Structures: Theory and Applications to Earthquake Engineering*, 4th ed.; Pearson Education: Upper Saddle River, NJ, USA, 2012.
42. Rybacki, E.; Jokisch, A.; Ziegenhagen, B.; Dresen, G.; Brantut, N.; Heidbach, O.; Meier, T. Semi-Brittle Deformation of Carrara Marble: Hardening and Strengthening Mechanisms in a Massive Carbonate Rock. *J. Geophys. Res. Solid Earth* **2021**, *126*, e2021JB022573. [CrossRef]
43. Mohr, O. Welche Umstände bedingen die Elastizitätsgrenze und den Bruch eines Materials? *Z. Ver. Dtsch. Ing.* **1900**, *44*, 1524–1530.
44. Martin, C.D.; Kaiser, P.K.; McCreath, D.R. Hoek-Brown parameters for predicting the depth of brittle failure around tunnels. *Can. Geotech. J.* **1999**, *36*, 136–151. [CrossRef]
45. Gullì, D.; Pellegri, M.; Marchetti, D. Mechanical behaviour of Carrara marble rock mass related to geo-structural conditions and in-situ stress. In Proceedings of the 8th South American Congress on Rock Mechanics: Integrating Innovation of Rock Mechanics, Buenos Aires, Argentina, 15–18 November 2015.
46. Cao, M.; Li, X.; Li, Y.; Wu, J.; Li, P.; Zhou, Y. Stress Characteristics and Mechanical Behavior of Rock Masses with an Opening under Complex Deep Underground Stress Conditions. *Appl. Sci.* **2024**, *14*, 7197. [CrossRef]
47. Shan, R.; Bai, H.; Li, Y.; Wu, H.; Sun, P.; Zhao, X.; Dou, H.; Wang, H. Analytical Solution of Surrounding Rock Stress and Plastic Zone of Rectangular Roadway under Non-Uniform Stress Field. *Sci. Rep.* **2024**, *14*, 27482. [CrossRef]
48. Lan, R.; Zhang, Z.; Wang, H.; Li, J.; Zou, Q.; Gao, F. The Influence of the Number of Free Surfaces on the Energy Distribution and Fragmentation Degree in Blasting of Hard Rock. *Front. Earth Sci.* **2023**, *11*, 1210650. [CrossRef]
49. Martin, C.D.; Christiansson, R.; Söderhäll, J. Stress Concentrations Caused by Sharp Corners and Large Regions of Low Confinement in Underground Openings. In *SKB Technical Report*; TR-01-38; Svensk Kärnbränslehantering AB: Stockholm, Sweden, 2001; Available online: https://skb.se/upload/publications/pdf/TR-01-38.pdf (accessed on 5 November 2025).
50. Lei, Q.; Latham, J.-P.; Xiang, J. Implementation of an Empirical Joint Constitutive Model into Finite-Discrete Element Analysis of the Geomechanical Behaviour of Fractured Rocks. *Rock Mech. Rock Eng.* **2016**, *49*, 4799–4816. [CrossRef]
51. Burjánek, J.; Gassner-Stamm, G.; Poggi, V.; Moore, J.R.; Fäh, D. Ambient Vibration Analysis of an Unstable Mountain Slope. *Geophys. J. Int.* **2010**, *180*, 820–828. [CrossRef]
52. Kleinbrod, U.; Burjánek, J.; Fäh, D. Ambient Vibration Classification of Unstable Rock Slopes: A Systematic Approach. *Eng. Geol.* **2019**, *249*, 198–217. [CrossRef]
53. McKinnon, S.D. Analysis of stress measurements using a numerical model methodology. *Int. J. Rock Mech. Min. Sci.* **2001**, *38*, 699–709. [CrossRef]